Journal of Non-Crystalline Solids 405 (2014) 163–169

Contents lists available at ScienceDirect

Journal of Non-Crystalline Solids

journal homepage: www.elsevier.com/ locate/ jnoncrysol

Monitoring crystallization in lithium silicate glass-ceramics using $^{7}Li \rightarrow {}^{29}Si$ cross-polarization NMR

Cornelia Schröder [a], Mariana de Oliveira Carlos Villas-Boas [b], Francisco C. Serbena [c], Edgar D. Zanotto [b], Hellmut Eckert [a,d,*]

[a] Institut für Physikalische Chemie, WWU Münster, Corrensstraße 30, D 48149 Münster, Germany
[b] Laboratório dos Materiais Vitreous (LaMaV), Universidade Federal em São Carlos, Rod. Washington Luis, km 235, C.P. 676 13.565-905, São Carlos, SP, Brazil
[c] Departamento de Física e Astronomia, Universidade Estadual de Ponta Grossa, CEP 84030-900 Ponta Grossa, PR, Brazil
[d] Instituto da Física em São Carlos, Universidade de São Paulo, Avenida Trabalhador Sãocarlense 400, CEP 13.566-590, São Carlos, SP, Brazil

ARTICLE INFO

Article history:
Received 8 July 2014
Received in revised form 2 September 2014
Accepted 8 September 2014
Available online xxxx

Keywords:
Lithium disilicate;
Glass ceramic;
NMR;
Crystalline fraction;
Cross-polarization

ABSTRACT

Quantification of the crystalline versus amorphous fraction is an important objective for the structural characterization of glass-ceramics. Owing to its well-documented ability of differentiating between crystalline and amorphous materials and its inherently quantitative character, magic-angle-spinning solid state nuclear magnetic resonance (MAS-NMR) spectroscopy is an excellent method for this objective. For the technologically important lithium disilicate glass-ceramics, the applicability of ^{29}Si MAS-NMR is, however, seriously impeded by poor signal to noise ratios and extremely long spin–lattice relaxation times (on the order of magnitude of hours). The detection sensitivity problem can be overcome by magnetization transfer from ^{7}Li nuclei to the ^{29}Si spins ($^{7}Li \rightarrow {}^{29}Si$ cross-polarization). While this method is inherently non-quantitative owing to the influence of various relaxation processes involved, we show that it can be successfully calibrated to yield quantitatively reliable crystalline fractions that are similar to those determined by alternative methods (optical microscopy and X-ray powder diffraction). In addition, this method can be used to detect very low (~1%) crystallized volume fractions.

1. Introduction

Owing to their relatively high fracture toughness (2.0–2.7 $MPa \times m^{1/2}$) and flexural strength (350–400 MPa), good chemical durability and low mass density, lithium disilicate glass-ceramics are among the top choices for transparent armor applications and restorative dentistry [1–5]. Their technological value arises from all the above positive combinations of properties plus the possibility of being prepared in opaque, translucent or transparent form, their easy formability into complex shapes and their moderate cost. The large aspect ratios of lithium disilicate crystals grown within the glassy matrix produce a microstructure ideal for crack deflection and toughening. Dental restorations fabricated with lithium disilicate based glass-ceramics currently represent a multimillion Euro market.

The development of new or improved lithium disilicate glass-ceramics requires a solid understanding of their mechanisms of crystallization, the rates of crystal nucleation and growth involved, and their impact on the nano- and microstructural organization. While X-ray diffraction methods remain the standard-bearer experimental tool for phase identification and structural characterization of well-ordered materials with high crystallinity, they are less well-suited for studying the *early nucleation* stages. Here modern magnetic resonance techniques offer powerful element-selective, inherently quantitative insights into structure and dynamics at the atomic scale [6]. For example, high-resolution $^{6/7}Li$ and ^{29}Si NMR have been widely applied for monitoring the formation of lithium disilicate-based glass ceramics [7–21]. While most of the results obtained indicate that stoichiometric disilicate glass transforms directly into the crystalline compound, there have been also some reports of metastable $Li_2Si_2O_5$ (and lithium metasilicate) precursor phases [9,12]. Furthermore, off-stoichiometric and/or P_2O_5-containing glasses – used in commercial glass-ceramics – result in the additional formation of crystalline phases of lithium metasilicate, lithium phosphate and quartz, accompanied by compositional changes in the residual glass matrix [7,15,20,21]. An accurate quantification of the crystalline content of lithium silicate glass-ceramics is severely hampered, however, by the low natural abundance of the ^{29}Si isotope and its relatively small gyromagnetic ratio ($\gamma = -5.319 \times 10^{6}\ T^{-1}\ rad\ s^{-1}$), resulting in low detection sensitivity. This problem is severely compounded by extremely long ^{29}Si spin–lattice relaxation times [8,21] – both for the glassy and the crystalline component – necessitating signal accumulation times on the order of one week per sample for building up sufficient signal to noise ratios suitable for quantitative analyses.

* Corresponding author at: Institut für Physikalische Chemie, WWU Münster, Corrensstraße 30, D 48149 Münster, Germany.
E-mail addresses: eckerth@uni-muenster.de, eckert@ifsc.usp.br (H. Eckert).

http://dx.doi.org/10.1016/j.jnoncrysol.2014.09.008
0022-3093/

In principle, significant gains in signal-to-noise ratio (and hence reduction in overall measurement time) may be achieved by means of cross-polarization (CP) methods, where the large magnetization of highly abundant nuclei with large magnetic moments is channeled to weakly abundant and/or low-gamma nuclei, and the signal is acquired under conditions of MAS (e.g. CPMAS-NMR) [22]. While the overwhelming majority of such applications involve magnetization transfer from ^{1}H to ^{13}C nuclei, we have recently reported analogous $^{7}Li \rightarrow {}^{29}Si$ cross-polarization experiments, resulting in significant signal-to-noise gains and spectral editing opportunities in the spectroscopy of various crystalline binary lithium silicides [23,24]. Part of the signal-to-noise benefit arises from the fact that in $^{7}Li \rightarrow {}^{29}Si$ cross-polarization the recycle delay used for signal accumulation depends on the spin–lattice relaxation time of the magnetization source nuclei (here ^{7}Li), which in general relax much faster than the ^{29}Si nuclei. On the other hand a serious drawback of cross-polarization methods is their generally non-quantitative character. Signal amplitudes generated by cross-polarization are affected by the influence of various superimposed relaxation processes involving the two spin systems and their surroundings, making it difficult to relate signal intensities to spin populations [25]. This complication is particularly serious for spin systems containing quadrupolar nuclei such as ^{7}Li, where population transfers among the different Zeeman levels during the MAS rotor period can interfere with spin locking [26–29].

In this contribution, we have addressed this challenge, developing a reliable $^{7}Li \rightarrow {}^{29}Si$ cross-polarization procedure for measuring crystallized volume fractions in lithium disilicate glass-ceramics. We validate our procedure by comparison with more established methods (optical microscopy and X-ray powder diffraction analyses) and discuss the advantages and limitations of the various methods to be used.

2. Fundamental concepts and methodology

Fig. 1 shows the pulse sequence used for the $^{7}Li \rightarrow {}^{29}Si$ CPMAS experiments in the present study. First, transverse ^{7}Li magnetization is prepared by a 90° pulse, which is subsequently fixed in the rotating frame by applying a 90° phase-shifted B_1 field. In this "spin locked" state, the ^{7}Li nuclei precess with their nutation frequency around the direction of the applied B_1 field perpendicular to the direction of the external magnetic field. During the "contact time" period t_c the ^{7}Li and ^{29}Si spins are simultaneously irradiated at their respective resonance frequencies. The radio frequency irradiation amplitudes B_1 of both spin species are chosen such that their respective precession frequencies in the doubly rotating frame are matched, following the Hartmann–Hahn condition [30], modulated by magic-angle spinning as given by [29]

$$\omega_1\left({}^{29}\mathrm{Si}\right) = \omega_1\left({}^{7}\mathrm{Li}\right) \pm n\omega_r \tag{1}$$

where $\omega_1(^{29}Si)$ and $\omega_1(^{7}Li)$ are the effective nutation angular frequencies of ^{29}Si and ^{7}Li and ω_r is the angular rotor frequency. For spin-1/2 nuclei such as ^{29}Si ω_1 is given by the product of $\gamma(^{29}Si) \times B_1(^{29}Si)$ where $\gamma(^{29}Si)$ is the gyromagnetic ratio of the ^{29}Si recipient nuclei. In the case of the quadrupolar ^{7}Li nuclei, the analogous situation $\omega_1(^{7}Li) = \gamma(^{7}Li) \times B_1(^{7}Li)$ holds only true if it is large compared to the quadrupolar angular frequency $\omega_Q(^{7}Li) = 3C_Q / 2I(2I-1)$, where C_Q and I are the ^{7}Li quadrupolar coupling constant and the spin quantum number (3/2), respectively. This situation corresponds to the non-selective excitation of all 2I Zeeman transitions. In the opposite extreme case, which corresponds to the selective excitation of the $m = 1/2 \leftrightarrow m = -1/2$ Zeeman transition, the effective nutation frequency is equal to $\omega_1 = (I + 1/2)\gamma B_1$. In the case of ^{7}Li, for which typical C_Q values are measured on the order of ~100 kHz, neither of these extremes is realized. As a result, an orientational distribution of nutation frequencies is observed, whose average adopts an intermediate value between the above extreme cases. As these distributions of nutation frequencies result in distributions of Hartmann–Hahn matching conditions, which are additionally modulated further by MAS according to Eq. (1), it is advantageous to subject the amplitude of the ^{7}Li spin-lock field to a linear ramping function [31]. With the ^{29}Si and ^{7}Li nuclei precessing with equal frequencies in the doubly rotating frame during the contact time period, magnetization transfer occurs via the ^{7}Li–^{29}Si magnetic dipole–dipole interaction between proximal nuclei, resulting in a significant boost of the ^{29}Si detection sensitivity. As discussed for the more common case of $^{1}H \rightarrow {}^{13}C$ CPMAS the optimal value chosen for the contact time, t_c, depends on the interplay of three competing rate constants (see Fig. 1) [25]: the cross-relaxation rate T_c^{-1} governing the magnetization transfer between the two spin systems, (2) the rotating frame spin–lattice relaxation rate of the source nuclei, $T_{1\rho}^{-1}(^{7}Li)$, describing the dispersal of their spin-locked magnetization, and (3) the rotating-frame spin lattice relaxation rate of the recipient nuclei, $T_{1\rho}(^{29}Si)$, describing the analogous process for the ^{29}Si magnetization created by $^{7}Li \rightarrow {}^{29}Si$ cross-relaxation during the contact time. While the first process favors increasing ^{29}Si magnetization buildup with increasing contact time, the latter two processes lead to signal diminution with increasing t_c. As a result, an optimum contact time exists, for which

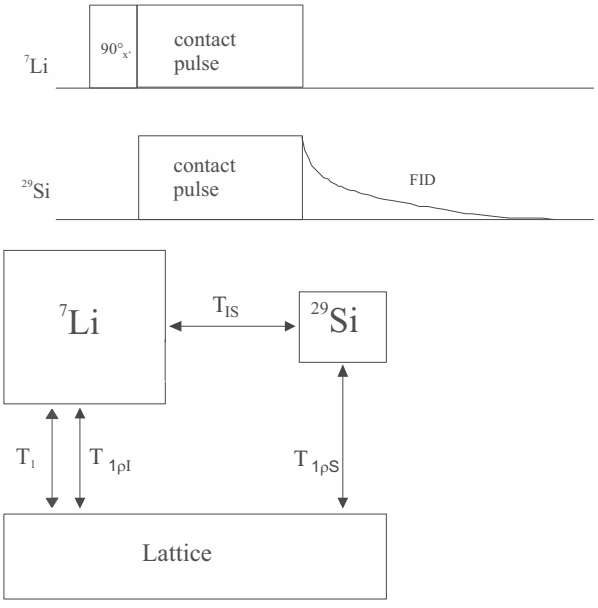

Fig. 1. Pulse sequence of the cross-polarization experiment and scheme illustrating the relaxation processes involved.

Fig. 2. Optical micrograph of a lithium disilicate glass-ceramic obtained by annealing glassy lithium disilicate for 90 h at 500 °C.

maximum signal amplitude is observed; this optimum time is usually determined empirically by variable contact time CP experiments. Various experimental protocols exist by means of which the three rate constants can be measured individually [25]. An additional complication arises if quadrupolar nuclei are involved, either as source or as recipient nuclei [26–29]. In this case one has to bear in mind that their rotating frame relaxation rates will be critically dependent on the value of B_1 chosen for the Hartmann–Hahn matching condition. The ability of spin-locking the transverse magnetization of quadrupolar nuclei is affected by population transfers between the various nuclear Zeeman states. Spin lock efficiency is controlled by the so-called adiabaticity parameter

$$\alpha = \frac{\omega_1^2}{\omega_Q \omega_{rot}} \tag{2}$$

and α values $\gg 1$ (*adiabatic* regime) or $\ll 1$ (*sudden* regime) are favorable for maintaining good spin-lock behavior. As both ω_1 and ω_r can be controlled experimentally, the first step in setting up cross-polarization experiments with quadrupolar nuclei is finding the optimum condition for spin-locking. This is best done by measuring $T_{1\rho}$ as a function of radio frequency power level at a fixed spinning frequency. Once this condition has been identified, the optimum value of t_c is determined by means of variable contact time experiments. Finally it must be kept in mind that the extent of magnetization transfer is also dependent on the total magnitude of the spin-locked magnetization of the source nuclei (here ^{7}Li). The latter depends on the recycle delay chosen for signal accumulation, in relation to the laboratory-frame spin–lattice relaxation time T_1 of the source nuclei.

For the analysis of phase mixtures (such as the crystalline and glassy components present in glass-ceramics) the above-discussed rate constants are generally different for the different phases, reflecting different spin dynamics. For this reason, optimum magnetization transfer conditions can usually be found only for one of the components in the phase mixture, and it would thus be unrealistic to attempt relative quantifications directly from the measured peak area ratios reflecting the individual components. A reliable quantification should be possible, however, by comparing the amplitude ratios observed in the analyte of interest with those of standard samples containing the individual components in known relative quantities. Thus, in our application to lithium disilicate glass-ceramics we can compare the ratio of the signal areas measured for the spectroscopically resolved resonances of the crystalline and the glassy component in a glass-ceramic with those of a corresponding calibration curve. The calibration curve is generated from a series of glass/crystal phase mixtures in which the respective quantities are well known. Of course, this approach assumes that the spin dynamics of the material does not depend on its physical state and/or thermal history. This question will be addressed in the present contribution.

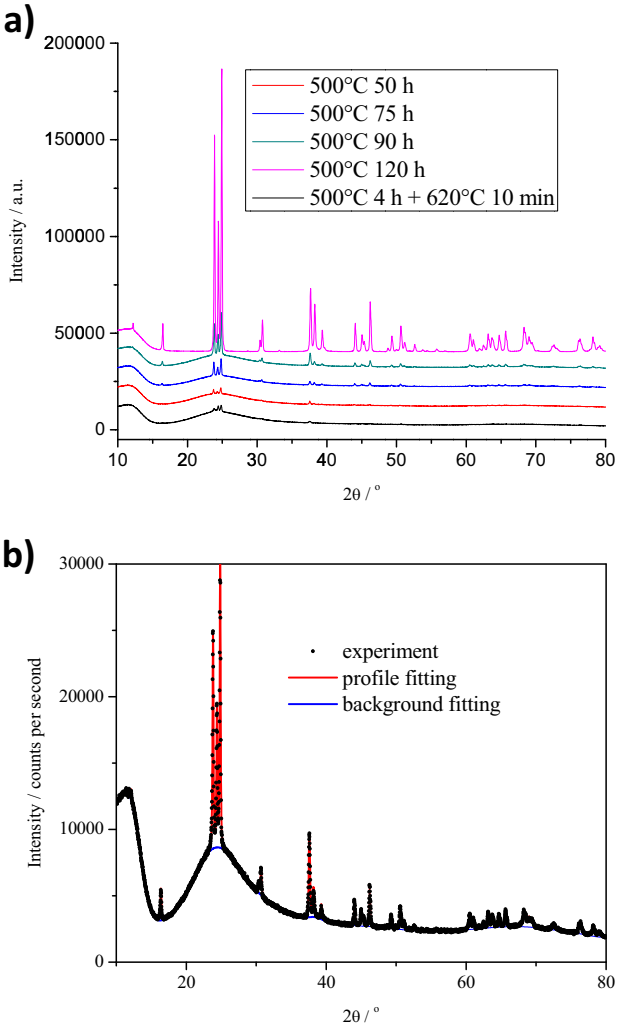

Fig. 3. a) X-ray powder diffractograms of a series of glass-ceramics obtained by successive annealing of glassy material under the conditions indicated. b) X-ray powder diffractogram of a sample annealed at 500 °C for 90 h and corresponding Rietveld fitting curve.

3. Experimental

3.1. Sample preparation and characterization

Lithium disilicate glass was prepared in 30 g quantity by heating stoichiometric homogeneous mixtures of lithium carbonate (99.0%), Synth, and silica (99.9999%), Santa Rosa, for 4 h at 1500 °C in a platinum crucible. Samples were rapidly quenched on a stainless steel block, and crushed and re-melted three times to ensure homogeneity. The glass transition temperature T_g obtained by the method of tangents was measured to be 452 °C, using a Netzsch STA 409 instrument operated at a heating rate of 10 °C/min. To produce glass-ceramics, the samples were annealed according to two distinct protocols: (A) single stage heat treatment at 500 °C for 50, 75, 90, and 120 h, respectively and (B) two stage treatment at 500 °C for 4 h (nucleation), followed by crystal growth treatments at 620 °C for 5, 10, and 20 min respectively. For comparison with the NMR spectroscopic data, the degree of crystallinity was also quantified by optical microscopy and X-ray powder diffraction. Microscopy was conducted on a LEICA DMRX optical microscope, operating at a resolution of ca. 10 μm. A typical result is shown in Fig. 2. Good

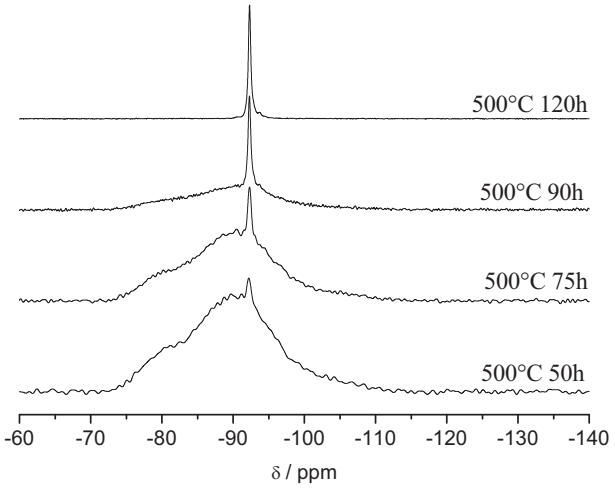

Fig. 4. ^{7}Li → ^{29}Si CPMAS NMR spectra of lithium disilicate glass-ceramics annealed at 500 °C for different annealing times.

contrast between the glassy and crystalline regions is obtained both in the transmission and the reflection modes, and crystallinity was quantified based on a comparison of relative areas in the reflection mode. Each value is the mean of at least 10 independent measurements.

X-ray diffraction (XRD) measurements were conducted using a RIGAKU ULTIMA IV diffractometer with a CuKα source in step scan mode. The 2θ range was from 6° to 80° or 120° at 0.018° intervals. The collection time at each step was set in order for the most intense peak in each diffractogram to reach 10,000 counts. All samples were measured in bulk form. The experimental data were subjected to a Rietveld analysis using the GSAS software [32] with the EXPGUI interface [33]. Typical results are presented in Fig. 3. For quantification of the crystalline phase, the areas under the background and under the peaks were fitted graphically and the crystallized volume fraction was estimated as the ratio $A_P/(A_P + A_B)$, where A_P and A_B are the sum of the peak area and the background area, respectively. The basic assumption of this method is that the radiation scattered by atoms is the same if it is in the amorphous or crystalline state and is well suited as the glass and crystalline phase is stoichiometric for this glass-ceramic and its density difference is small. We use the same temperature factors of the atoms of the unit cell for all the refinements. We performed the calculation of crystallized volume fractions for the intervals 6°–80° and 6°–120° and no significant differences were found between them. The reported results are those calculated for the 6°–80° interval. The difference in the unit cell volume by Rietveld analysis was found to be no more than 0.2% for all samples analyzed when compared with the fully crystallized sample.

3.2. Solid state NMR

All the solid state NMR measurements were conducted on a Bruker DSX 400 MHz spectrometer, equipped with 4.0 mm double and triple resonance magic angle spinning probes. ^{7}Li single pulse spectra were recorded using 90° pulses of 2.8 μs and a relaxation delay of 10 s. Spin–lattice relaxation times were measured by the saturation recovery sequence. For the ^{7}Li → ^{29}Si CPMAS NMR studies, the following measurement conditions were applied: ^{7}Li 90° pulse length 4.5 μs, spinning frequency 8.0 kHz, contact time 9.0 ms, and relaxation delay 5 s. The radio frequency amplitude on the ^{7}Li channel was varied between 50 and 100%, using a linear ramp that was optimized automatically to yield maximum signal-to-noise ratio [31]. All the ^{29}Si NMR spectra are referenced against tetramethylsilane ($SiMe_4$) at 0 ppm.

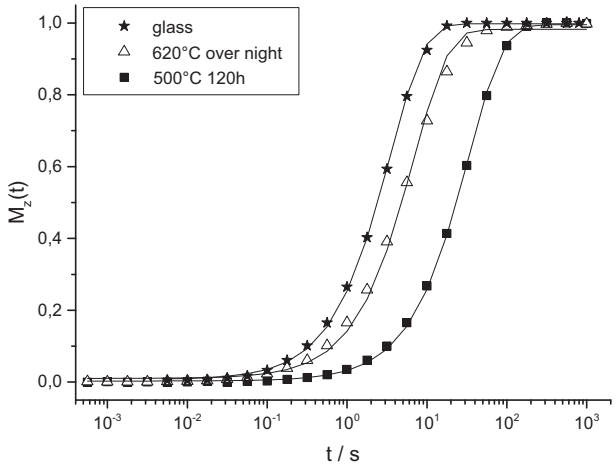

Fig. 5. ^{7}Li saturation recovery curves measured for lithium disilicate glass and for two fully crystallized samples of $Li_2Si_2O_5$. Solid curves show fits of the experimental data to mono-exponential recovery functions, given by $M = M_0(1 - \exp - t / T_1)$, resulting in best-fit values of 3.5 s, 6.9 s, and 33.7 s for glassy lithium disilicate, $Li_2Si_2O_5$ crystallized at 620 °C, and $Li_2Si_2O_5$ crystallized at 500 °C, respectively.

4. Results and discussion

4.1. ^{7}Li → ^{29}Si cross-polarization spectra

Fig. 4 shows ^{7}Li → ^{29}Si cross-polarization spectra obtained on a series of glass-ceramics annealed at 500 °C for different annealing times. Acceptable signal to noise ratio can be attained with ~14,200 scans, requiring total measurement times on the order of ~20 h. The crystalline material is easily identified by a sharp resonance signal at −92.4 ppm ($Q^{(3)}$ units) whereas the broader component comprises the resonances of $Q^{(2)}$, $Q^{(3)}$ and $Q^{(4)}$ units of the glassy material. These signal components are identical to the ones measureable by ^{29}Si single pulse MAS-NMR (with vastly higher investments in measurement time), indicating that all types of $Q^{(n)}$ species are effectively detected by CPMAS under these conditions. Quantification of the crystalline material by straightforward lineshape analysis of the spectra in Fig. 4, is, however, not possible, because the relative signal intensities for both the crystalline and the glassy components are strongly affected by the above-described three types of relaxation processes (see Fig. 1). In the following, we will show that by accounting for these effects with a suitable calibration procedure, reliable quantitative ratios of crystalline versus amorphous material can be obtained.

4.2. ^{7}Li spin–lattice relaxation

Fig. 5 compares the ^{7}Li saturation recovery curves of lithium disilicate glass with those of the two fully crystallized $Li_2Si_2O_5$ samples. The data are well-approximated by mono-exponential relaxation behavior, $M = M_0(1 - \exp - t / T_1)$, where T_1 is the laboratory-frame spin–lattice relaxation time describing the rate of this recovery process and M_0 is the equilibrium magnetization measured at $t > 5 \times T_1$. We determine T_1 values of 3.5 s, 6.9 s, and 33.7 s for glassy lithium disilicate, $Li_2Si_2O_5$ crystallized at 620 °C, and $Li_2Si_2O_5$ crystallized at 500 °C, respectively. In particular, the large difference in T_1 values measured for the two crystallized lithium disilicate samples is unexpected and must be taken into consideration for the analysis of crystallinity. In all the measurements done with ^{7}Li relaxation delays smaller than 5 times the longest spin–lattice relaxation time present in the sample, the slower-relaxing crystalline fraction will be consistently *under-estimated*, as the fraction of the ^{7}Li magnetization spin-locked under such conditions will be lower than that for the glassy material. From the above

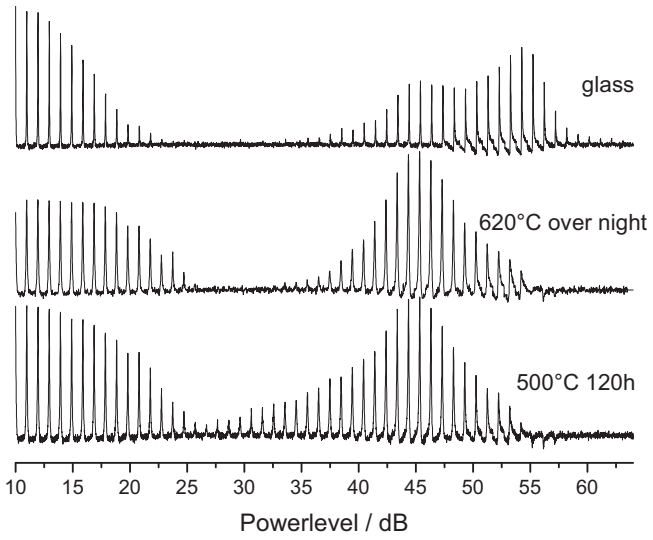

Fig. 6. Dependence of ^{7}Li signal amplitude on the radio frequency amplitude, expressed in terms of power attenuation level (dB) adjusted at the spectrometer. Each signal is obtained for a ^{7}Li 90° preparation pulse of 4.8 μs length, a spinlock time of 10 ms and represents the average of 12 scans.

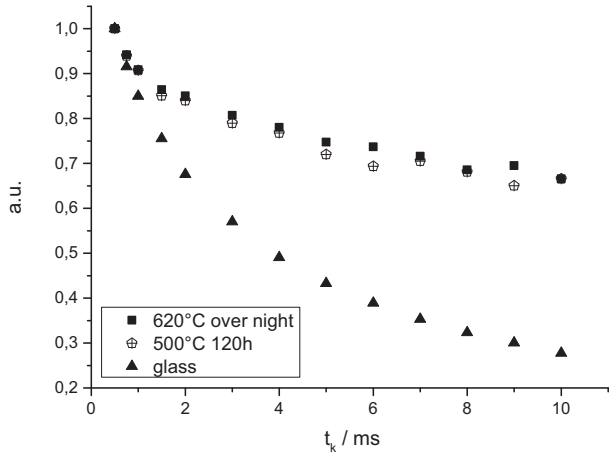

Fig. 7. Decay of ^{7}Li spin-locked transverse magnetization as a function of spin-lock duration, measured at a ^{7}Li nutation frequency of 28.0 kHz.

results, it is clear that the effect will be significantly more serious in the samples crystallized at 500 °C than in those crystallized at 620 °C.

4.3. ^{7}Li rotating-frame relaxation (spin-lock behavior)

Fig. 6 shows stack plots of ^{7}Li signal amplitudes generated by a 4.8 μs 90° pulse, followed by a 10 ms spin locking time under variation of the radio frequency power level of the spin-lock pulse applied, for both of the two fully crystallized lithium disilicate samples and for the fully glassy material. The signal amplitudes measured in these experiments characterize the efficiency of spin-locking under these conditions, which is a pre-requisite for successful cross-polarization experiments. The power level, which is a measure of the quantity ω_1, is specified here in terms of the attenuation level selected at the spectrometer, high values corresponding to low output power. Fig. 6 illustrates the two distinct radio-frequency power regimes available for obtaining good ^{7}Li spin-lock conditions. The low attenuation levels (high ^{7}Li rf power and ω_1 values) correspond to the *adiabatic* regime, whereas the high attenuation levels (low ^{7}Li rf power and ω_1 values) correspond to the *sudden* regime. Fig. 6 implies that in the *sudden* regime favorable signal amplitudes are only attainable at impractically low radio frequency power levels corresponding to 90° pulse lengths exceeding 100 μs. Based on these results, the *adiabatic* regime is chosen for the ^{7}Li → ^{29}Si cross-polarization experiments in the present study. Thus, the CPMAS spectra shown in Fig. 4 were recorded at a nutation frequency of $\omega_1 = 2\pi \times 28.0$ kHz (output power attenuation level 10 dB). To select the most suitable contact time, it is important to study the dependence of signal amplitude on spin lock duration at the radio frequency amplitude chosen. These results are summarized in Fig. 7. For the two crystallized samples the decay is non-exponential in character, but the ^{7}Li nuclei in them show essentially identical spin-lock behavior. In contrast, the glassy sample shows an exponential relaxation behavior in the rotating frame, with a substantially faster decay compared to the crystalline samples. With the experimental conditions (ω_1 and ω_r) kept constant, differences between the adiabaticity parameters between crystalline and glassy samples must be attributed to differences in ω_Q. Indeed, Fig. 8 confirms that glassy lithium disilicate has a larger ^{7}Li quadrupolar coupling constant than the crystalline materials: the spinning sideband manifolds reflecting the modulated $|m| = 1/2 \leftrightarrow |m| = 3/2$ satellite transitions extend over a significantly wider frequency range. From these data we estimate C_Q (^{7}Li) = 180 ± 20 kHz and 280 ± 20 kHz for crystalline lithium disilicate and glassy lithium disilicate, respectively. As a consequence, in the adiabatic regime α (c-$Li_2Si_2O_5$) > α (g-$Li_2Si_2O_5$), resulting in a more efficient spin-lock for the crystalline material. Based on these considerations the CPMAS experiment is expected to lead to a systematic *over-estimation* of the crystalline fraction.

4.4. External calibration

Fig. 9 shows a plot of the ^{7}Li → ^{29}Si CP-MAS fractional signal area attributed to crystalline lithium disilicate for a series of physical mixtures of glassy lithium disilicate and crystalline lithium disilicate, obtained by heating at 620 °C. Clearly, under the experimental conditions chosen (nutation angular frequency $2\pi \times 28$ rad s^{-1}, contact time 9 ms, relaxation delay 5 s) the crystalline fraction is over-estimated. This result indicates that the relative attenuation of the spin-lock signal of the crystalline fraction due to the longer spin–lattice relaxation time effect is over-compensated by its much higher spin-lock efficiency. Nevertheless, this curve can now be used as a calibration curve to obtain accurate crystalline fractions in partially ceramized samples. The results are summarized in Table 1. The crystalline fractions obtained for the three glass-ceramics obtained by two-stage annealing are in very good agreement with the results from optical microscopy and X-ray diffraction. In contrast, when this calibration curve is applied to glass-ceramics annealed at 500 °C, huge deviations are observed (see values in parentheses given in Table 1). These deviations are caused by the much longer spin–lattice relaxation time of the lithium disilicate crystallized at 500 °C. As illustrated in Fig. 10, however, this problem can be solved by choosing a fully crystalline lithium disilicate sample obtained at 500 °C for the calibration mixture. The different calibration curve obtained for this mixture arises from the fact that the spin–lattice relaxation time of crystalline $Li_2Si_2O_5$ obtained at 500 °C is substantially

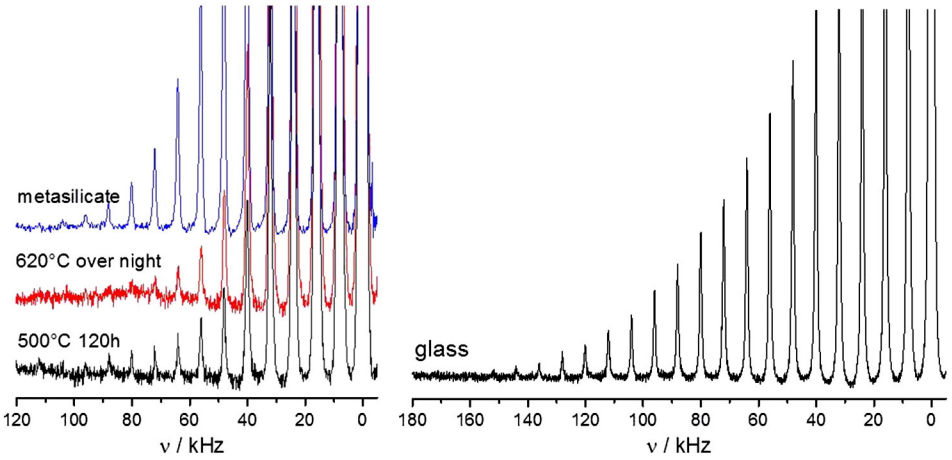

Fig. 8. Vertically expanded ^{7}Li satellite transition (SATRAS) MAS-NMR spectra of fully crystalline lithium metasilicate (left, top), two samples of crystalline lithium disilicate crystallized at different temperatures (left, middle and bottom) and of glassy lithium disilicate (right). In each plot, the peak at the lowest frequency shown corresponds to the central Zeeman transition.

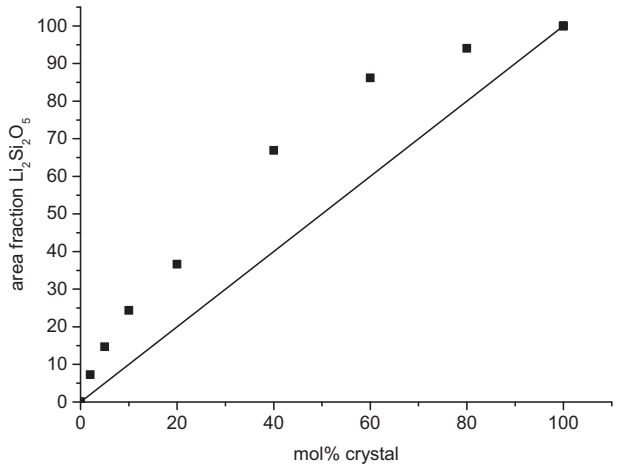

Fig. 9. $^{7}Li \rightarrow {}^{29}Si$ CPMAS calibration curve for lithium disilicate glass-ceramics obtained with a 5 s relaxation delay: Fractional signal area of the crystalline component versus crystalline content in physical mixtures of glassy lithium disilicate and fully crystalline material obtained at 620 °C. The solid line shows the identity.

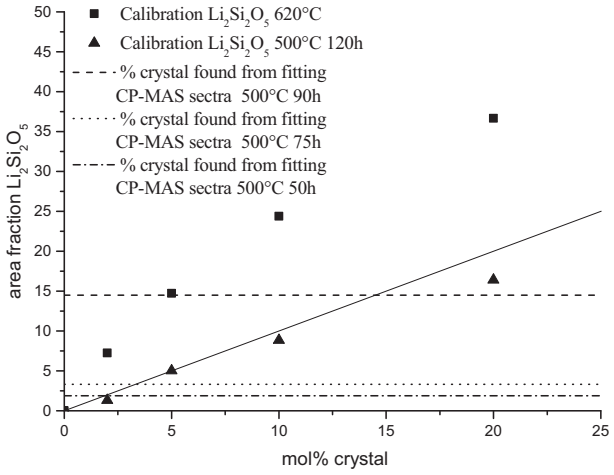

Fig. 10. Calibration curve of Fig. 9 (squares) and new calibration curve based on crystalline samples obtained under the identical experimental conditions by using physical mixtures of glassy lithium disilicate and fully crystalline material obtained at 500 °C (triangles). The crystalline fractions deduced from each calibration curve for the three analyte samples of Fig. 4 are given by the intersections of the horizontal dashed lines with the respective calibration curves. The solid line shows the identity.

longer; therefore, the amplitude of spin-locked ^{7}Li transverse magnetization arising from crystalline $Li_2Si_2O_5$ (relative to that arising from the glassy component) is substantially smaller than with the set of samples heated at 620 °C (Fig. 9). We further verified that by choosing a ^{7}Li relaxation delay that is at least 5 times the longest relaxation time in the sample under study (180 s in the present case), identical calibration curves are obtained with both sets of samples. Ideally, these quantification experiments should always be done under such conditions, when unknown samples are being studied. The ^{7}Li spin–lattice relaxation times in such samples can be subject to large variations as they are strongly influenced by the level of paramagnetic impurities present, which may partition differently between crystalline and glassy phases at different annealing temperatures. Therefore, in samples of uncertain batch origins and thermal histories the spin–lattice relaxation times must always be measured beforehand, and the quantification must be conducted using a relaxation delay of five times T_1. The faster (and hence preferable) steady-state conditions, where there is no full relaxation, but the signal per pulse is the same because of constant partial saturation of the magnetization, lead to maximum signal amplitude per unit time for recycle delays ~1 times T_1. Studies under such conditions are reliable only if one ensures that the crystalline material that is used in the calibration sample originates from the same batch and has been treated at the same temperature as the analyte ceramic sample under study.

5. Conclusions

In summary, the results of the present study show that $^{7}Li \rightarrow {}^{29}Si$ CPMAS NMR experiments can be used to measure the fractions of crystalline and glassy components in lithium disilicate glass-ceramics, yielding results that are consistent with those obtained by the more established methods of optical microscopy and X-ray powder diffraction. As CPMAS NMR is inherently non-quantitative, the method needs to be calibrated, taking into account the different ^{7}Li NMR spin–lattice relaxation characteristics of the crystalline and glassy fractions. The results of the present study show that under adiabatic spin-locking conditions, the ^{7}Li spin-lock efficiency is higher for the crystalline component than for the glassy material, and this will lead to an over-estimation of the crystalline content, if no calibration is done. The rotating frame relaxation times ($T_{1\rho}$) of the crystallized materials, do, however, not depend on their crystallization temperatures. In contrast, the laboratory-frame ^{7}Li spin lattice relaxation times T_1 of crystalline lithium disilicate samples depend strongly on the annealing temperatures applied. For these reasons, the calibration curves and the measurements should be ideally done using relaxation delays in excess of 5 times the longest relaxation time present in these samples. As the latter may turn out impractical (as in the present case), the crystalline material to be used for the calibration curve should be obtained at the same annealing temperature as the temperature at which the analyte samples are generated. One further note of caution must be added: in phase separated glassy and glass-ceramic samples the method is not applicable if one of the phase constituents does not contain lithium. For such samples, which e.g. include high-silica (>75% SiO_2) lithium silicate glasses and ceramics there is no alternative to quantitative ^{29}Si Bloch-decay studies.

Overall, $^{7}Li \rightarrow {}^{29}Si$ CPMAS NMR represents a new NMR approach towards the structural and mechanistic study of lithium silicate based glass-ceramics. As the method has an enhanced detection sensitivity for the crystalline fraction compared to the glassy fraction, it will be particularly suitable for studies of the early nucleation and crystallization stages. At low volume fractions, this method may be superior to optical microscopy and XRD, particularly in cases where the nuclei have sizes below 1 μm, the resolution limit of optical microscopes or below 100 nm, where X-ray diffraction peaks become severely broadened. Early nucleation stages are also particularly interesting from a mechanistic point of view, as there have been various reports on crystalline precursor phases in this regime, whose role in the ceramization process has remained uncertain to date [34–36]. In the present study, our NMR results show no evidence for metastable precursor phases. Further application of this powerful technique towards nucleation and growth studies in non-stoichiometric and multi-component lithium silicate glasses are currently in progress.

Table 1
Crystalline fraction f_c (in percent) of lithium disilicate glass-ceramics obtained via calibrated NMR, optical microscopy and XRD Rietveld analysis.

Sample treatment	f_c (NMR)	f_c (microscopy)	f_c (XRD)
500 °C, 50 h	2.5 (0.4)[a]	1.9	1.0
500 °C, 75 h	3.8 (0.8)	4.9	3.0
500 °C, 90 h	15 (4.8)	9.4	6.7
500 °C, 120 h	100	n.d.[b]	n.d.
500 °C, 4 h + 620 °C, 5 min	0.0	0.0	n.d.
500 °C, 4 h + 620 °C, 10 min	2.1	2.2	1.0
500 °C, 4 h + 620 °C, 20 min	82	75	n.d.

[a] Values in parentheses denote fractions determined using the calibration curve based on a crystalline lithium disilicate sample obtained at 620 °C.
[b] n.d. = not determined.

Acknowledgments

The authors acknowledge financial support by the Brazilian funding agencies São Paulo Research Foundation (FAPESP) (CEPID Project 2013/07793-6) and CNPq (Universal Project 477053/2012-2).

References

[1] E.D. Zanotto, Am. Ceram. Soc. Bull. 89 (2010) 19.
[2] M.R. Fernandes, D.U. Tulyganov, M.J. Pascual, J.M.F. Ferreira, Ceram. Int. 40 (2014) 129.
[3] I. Denry, J.A. Holloway, Materials 3 (2010) 351.
[4] G.P. Ho, J.P. Matinlinna, Silicon 3 (2011) 109.
[5] E.D. Zanotto, Int. J. Appl. Glas. Sci. 4 (2013) 105.
[6] M. Edén, Ann. Rep. Prog. Chem. C 108 (2012) 77.
[7] C.M. Schramm, B.H.W.S. de Jong, V.E. Parziale, J. Am. Chem. Soc. 106 (1984) 4396.
[8] C.N.R. Rao, J.M. Thomas, J. Klinowski, U. Selvaraj, K.J. Rao, G.R. Millward, Angew. Chem. Int. Ed. 97 (1985) 56.
[9] R. Dupree, D. Holland, M.G. Mortuza, J. Non-Cryst. Solids 116 (1990) 148.
[10] D. Holland, Y. Iqbal, P. James, W.E. Lee, J. Non-Cryst. Solids 232–234 (1998) 140.
[11] Y. Iqbal, W.E. Lee, D. Holland, P.F. James, J. Mater. Sci. 34 (1999) 4399.
[12] Y. Iqbal, W.E. Lee, D. Holland, P.F. James, J. Non-Cryst. Solids 224 (1998) 1.
[13] J.W. Adams, S.R. Elliott, in: D.L. Pye, W.C. LaCourse, H.J. Stevens (Eds.), Phys. Non-Cryst. Solids, 1992, p. 742.
[14] D.J.M. Burkhard, G. Nachtegaal, J. Non-Cryst. Solids 209 (1997) 299.
[15] M.G. Mortuza, M.R. Ahasan, R. Dupree, D. Holland, J. Mater. Sci. 42 (2007) 7950.
[16] B. Zhang, A.J. Eastedal, N.R. Edmonds, D. Bhattacharyya, J. Am. Ceram. Soc. 90 (2007) 1592.
[17] A. Ananthanarayanan, G.P. Kothial, L. Montagne, B. Revel, J. Solid State Chem. 183 (2010) 1416.
[18] J.G. Longstaffe, U. Werner-Zwanziger, J.F. Schneider, M.L.F. Nascimento, E.D. Zanotto, J.W. Zwanziger, J. Phys. Chem. 112 (2008) 6151.
[19] M.D. O'Donnell, R.G. Hill, N. Karpukhina, G.V. Law, Dent. Mater. 27 (2011) 990.
[20] W. Höland, V. Rheinberger, E. Apel, Ch. Ritzberger, H. Eckert, C. Mönster, Phys. Chem. Glasses Eur. J. Glass Sci. Technol. B 48 (2007) 97.
[21] C. Bischoff, H. Eckert, E. Apel, V.M. Rheinberger, W. Höland, Phys. Chem. Chem. Phys. 13 (2011) 4540.
[22] J. Schaefer, E.O. Stejskal, J. Am. Chem. Soc. 98 (1976) 1031.
[23] S. Dupke, T. Langer, R. Pöttgen, M. Winter, H. Eckert, Solid State Nucl. Magn. Reson. 43 (2012) 17.
[24] S. Dupke, T. Langer, R. Pöttgen, M. Winter, S. Passerini, H. Eckert, Phys. Chem. Chem. Phys. 14 (2012) 6496.
[25] M. Duer, Introduction to Solid State NMR Spectroscopy, Wiley-Blackwell, 2005, ISBN 978-1-4051-0914-7. (and references therein).
[26] A.J. Vega, J. Magn. Reson. 96 (1992) 50.
[27] A.J. Vega, Solid State Nucl. Magn. Reson. 1 (1992) 16.
[28] S. Puls, H. Eckert, J. Phys. Chem. B 110 (2006) 14253.
[29] S.M. de Paul, M. Ernst, J.S. Shore, J.F. Stebbins, A. Pines, J. Phys. Chem. B 101 (1997) 3240.
[30] S.R. Hartmann, E.I. Hahn, Phys. Rev. 128 (1962) 2042.
[31] G. Metz, X.L. Wu, S.O. Smith, J. Magn. Reson. A 110 (1994) 219.
[32] A.C. Larson, R.B. Von Dreele, General Structure Analysis System (GSAS), Los Alamos National Laboratory Report LAUR 86-748, 2004.
[33] B.H. Toby, EXPGUI, a Graphical User Interface for GSAS, J. Appl. Crystallogr. 34 (2001) 210–213.
[34] P.C. Soares, E.D. Zanotto, V.M. Fokin, H. Jain, J. Non-Cryst. Solids 331 (2003) 217.
[35] E.D. Zanotto, J. Non-Cryst. Solids 219 (1997) 42.
[36] L.L. Burgner, P. Lukas, M.C. Weinberg, P.C. Soares, E.D. Zanotto, J. Non-Cryst. Solids 274 (2000) 188.